Published in final edited form as:
Nano Lett. 2013 June 12; 13(6): 2634–2639. doi:10.1021/nl4007744.

3D Printed Bionic Ears

Manu S. Mannoor[†], **Ziwen Jiang**[†], **Teena James**[§], **Yong Lin Kong**[†], **Karen A. Malatesta**[†], **Winston O. Soboyejo**[†], **Naveen Verma**[‡], **David H. Gracias**[§], and **Michael C. McAlpine**[†,*]

[†]Department of Mechanical and Aerospace Engineering, Princeton University, Princeton, NJ 08544

[§]Department of Chemical and Biomolecular Engineering, Johns Hopkins University, Baltimore, MD 21218

[‡]Department of Electrical Engineering, Princeton University, Princeton, NJ 08544

Abstract

The ability to three-dimensionally interweave biological tissue with functional electronics could enable the creation of bionic organs possessing enhanced functionalities over their human counterparts. Conventional electronic devices are inherently two-dimensional, preventing seamless multidimensional integration with synthetic biology, as the processes and materials are very different. Here, we present a novel strategy for overcoming these difficulties via additive manufacturing of biological cells with structural and nanoparticle derived electronic elements. As a proof of concept, we generated a bionic ear via 3D printing of a cell-seeded hydrogel matrix in the precise anatomic geometry of a human ear, along with an intertwined conducting polymer consisting of infused silver nanoparticles. This allowed for *in vitro* culturing of cartilage tissue around an inductive coil antenna in the ear, which subsequently enables readout of inductively-coupled signals from cochlea-shaped electrodes. The printed ear exhibits enhanced auditory sensing for radio frequency reception, and complementary left and right ears can listen to stereo audio music. Overall, our approach suggests a means to intricately merge biologic and nanoelectronic functionalities via 3D printing.

Keywords

Cybernetics; tissue engineering; bioelectronics; cyborg organs; electronic implants; additive manufacturing

The design and implementation of bionic organs and devices that enhance human capabilities, known as cybernetics, has been an area of increasing scientific interest.[1,2] This field has the potential to generate customized replacement parts for the human body, or even create organs containing capabilities beyond what human biology ordinarily provides. In particular, the development of approaches for the direct multidimensional integration of functional electronic components with biological tissue and organs could have tremendous impact in regenerative medicine, prosthetics, and human-machine interfaces.[3,4] Recently, several reports have described the coupling of electronics and tissues using flexible and/or stretchable planar devices and sensors that conform to tissue surfaces, enabling applications such as biochemical sensing and probing of electrical activities on surfaces of the heart,[5]

*Corresponding author, Telephone number: (609) 542-0275, mcm@princeton.edu.

SUPPORTING INFORMATION AVAILABLE:
Additional experimental details with materials, methods, and figures. This material is available free of charge at http://pubs.acs.org.

lungs,[6] brain,[7] skin[8] and teeth.[9] However, attaining seamless three dimensionally entwined electronic components with biological tissues and organs is significantly more challenging.[4]

Tissue engineering is guided by the principle that a variety of cell types can be coaxed into synthesizing new tissue if they are seeded onto an appropriate three-dimensional hydrogel scaffold within an accordant growth environment.[10–15] Following *in vivo* or *in vitro* culture, tissue structures form which possess the morphology of the original scaffold.[16] However, a major challenge in traditional tissue engineering approaches is the generation of cell-seeded implants with structures that mimic native tissue, both in anatomic geometries and intra-tissue cellular distributions.[17] Techniques such as seeding cells into nonadhesive molds or self-folding scaffolds have been used to fabricate three-dimensional tissue constructs with complex 3D geometries.[18,19] Yet, existing techniques are still incapable of easily creating organ or tissue parts with the required spatial heterogeneities and accurate anatomical geometries to meet the shortage of donor organs for transplantation.[20–22] For instance, total external ear reconstruction with autogenous cartilage – with the goal of re-creating an ear that is similar in appearance to the contralateral auricle – remains one of the most difficult problems in the field of plastic and reconstructive surgery.[23]

Additive manufacturing techniques such as 3D printing offer a potential solution via the ability to rapidly create computer-aided design (CAD) models by slicing them into layers and building the layers upwards using biological cells as inks, in the precise anatomic geometries of human organs.[24–27] Variations of 3D printing have been used as methods of solid freeform fabrication, although its use has mainly been limited to the creation of passive mechanical parts.[24,28] Extrusion-based 3D printing has been used to engineer hard tissue scaffolds such as knee menisci and intervertebral discs complete with encapsulated cells.[29–31] This technique offers the ability to create spatially heterogeneous multi-material structures by utilizing deposition tools that can extrude a wide range of materials.[32] Further, nanoscale functional building blocks enable versatile bottom-up assembly of macroscale components possessing tunable functionalities. This could allow for the simultaneous printing of nanoelectronic materials and biological cells to yield three dimensionally integrated cyborg tissues and organs exhibiting unique capabilities.[33,34]

Here we introduce a conceptually new approach that addresses the aforementioned challenges by fully interweaving functional electronic components with biological tissue via 3D printing of nanoelectronic materials and viable cell-seeded hydrogels in the precise anatomic geometries of human organs. Since electronic circuitry is at the core of sensory and information processing devices,[35] *in vitro* culturing of the printed hybrid architecture enables the growth of “cyborg organs” exhibiting enhanced functionalities over human biology. Our approach offers the ability to define and create spatially heterogeneous constructs by extruding a wide range of materials in a layer-by-layer process until the final stereolithographic geometry is complete. This concept of 3D printing of living cells together with electronic components and growing them into functional organs represents a new direction in merging electronics with biological systems. Indeed, such cyborg organs are distinct from either engineered tissue or conformal planar/flexible electronics and offer a unique way of attaining a three dimensional merger of electronics with tissue.

As a proof of concept of this approach, we evaluated the ability of 3D printing to create a viable ear auricle which also contains electronics that enable alternative capabilities to human hearing. Human organs comprising predominantly of cartilaginous tissue, such as the ear auricle, represent suitable prototype candidates to investigate the feasibility of our approach. This is due to 1) the inherent complexity in the ear’s anatomical geometry, which renders it difficult to bioengineer via traditional tissue engineering approaches, as well as 2) the simplicity in its cartilage tissue level structure due to the lack of vasculature.[23,36]

Additionally, bottom-up assembly of nanoelectronic matrices provides the ability to hierarchically generate functional macroscale electronic components. Specifically, we demonstrate 3D printing of a chondrocyte seeded alginate hydrogel matrix with an electrically conductive silver nanoparticle (AgNP) infused inductive coil antenna, connecting to cochlea-shaped electrodes supported on silicone. Taken together, the result is three dimensional integration of functional electronic components within the complex and precise anatomic geometry of a human ear (Fig. 1).

The following steps are involved in the process. First, a CAD drawing of the bionic ear (Fig. 1A) is used to prescribe the anatomic geometry and the spatial heterogeneity of the various functional materials. As described above, three materials comprise the three functional constituents (structural, biological, and electronic) of the bionic ear. These materials are fed into a syringe extrusion based Fab@Home 3D printer (The NextFab Store, Albuquerque, NM) (Fig. 1B). The printed bioelectronic hybrid ear construct is then cultured *in vitro* to enable cartilage tissue growth to form a cyborg ear with the capability of sensing electromagnetic signals in the radio frequency (RF) range by means of an inductive coil acting as a receiving antenna (Figure 1C).

To demonstrate our approach, we printed the bionic ear construct as follows. For the scaffold, we pre-seeded an alginate hydrogel matrix with viable chondrocytes at a density of ~60 million cells/mL (See Supporting Information). Alginate matrix is three dimensionally stable in culture, non-toxic, pre-seeding and extrusion compatible, and a suitable cell delivery vehicle because crosslinking can be initiated prior to deposition.[37] Chondrocytes used for the printing were isolated from the articular cartilage of one month old calves (Astarte Biologics, Redmond, WA). A CAD drawing of a human ear auricle in stereolithography format (STL) with an integrated circular coil antenna connected to cochlea shaped electrodes was used to define the print paths by slicing the model into layers of contour and raster fill paths. Crosslinking was initiated in the alginate hydrogel matrix pre-seeded with viable chondrocytes, which was then 3D printed along with conducting (AgNP-infused) and non-conducting silicone solutions (Movie 1). Together, this method produced the biological, electronic and structural components of the bionic organ in a single process.

Figure 2A shows the 3D printed bionic ear immediately after printing. Notably, it is found to faithfully reproduce the CAD drawing, in the precise spatiality for each material as dictated by the design. The printed ear construct was immersed in chondrocyte culture media containing 10% or 20% fetal bovine serum (FBS), which was refreshed every 1–2 days (See Supporting Information). The hybrid ear showed good structural integrity and shape retention under culture (Fig. 2B). Over time, the construct gradually became more opaque; this was most apparent after four weeks of culture, and is grossly consistent with developing an extracellular matrix (ECM). The gross morphology of the bionic ear after 10 weeks of *in vitro* culture is shown in the Supporting Information.

Viability was tested immediately before and during the various stages of the printing process. Initial viability of cells was determined after culturing using a Trypan blue cell exclusion assay (Corning Cellgrow, Mediatech, VA) and was found to be 96.4 ± 1.7% (Fig. 2C) (See Supporting Information). The printed cell-seeded alginate ear was also tested with a LIVE/DEAD® Viability Assay (Molecular Probes, Eugene, OR) and exhibited a cell viability of 91.3 ± 3.9% with homogeneous chondrocyte distribution. This result suggests that the printing process, including cell encapsulation and deposition, does not appreciably impact chondrocyte viability.

Notably, this approach of printing a pre-seeded hydrogel matrix eliminates the major problems associated with seeding depth limitations and non-uniform seeding in traditional

methods for seeding premolded 3D scaffolds. Seeding chondrocytes into a bioabsorbable alginate matrix and shaping it via 3D printing localizes the cells to a desired geometry, allowing for new ECM production in defined locations when cultured in nutritive media. As tissue develops, the polymer scaffold is reabsorbed (Fig. 2D), so that the new tissue retains the shape of the polymer in which the cells were seeded. The biodegradable scaffolding provides each cell with better access to nutrients and more efficient waste removal.

Next, histologic evaluation was used to compare the morphology of chondrocytes in the neocartilage of the bionic ear to that of the native cartilaginous tissue. Hematoxylin and eosin (H&E) staining revealed uniform distribution of the chondrocytes in the constructs (Fig. 2E) (See Supporting Information). Histology of the ear tissue with Safranin O staining indicated relatively uniform accumulation of proteoglycans in the cultured ear tissue (Fig. 2F). These biochemical data are consistent with the development of new cartilage.[38] Finally, fluorescent measurements were used to ascertain the viability of the 3D printed bionic ear tissue after 10 weeks of *in vitro* growth culture using fluorescein diacetate (FDA) and propidium iodide (PI) stains. Figures 2G and 2H show the tissue covering the coil antenna and the internal tissue that is in contact with the electrode that runs perpendicular through the tissue, respectively. In both cases, the grown cartilage exhibited excellent morphology and tissue level viability. Notably, this approach of culturing tissue in the presence of abiotic electronic materials could minimize the immune response of the grown tissue.

We then characterized the mechanical properties of the cartilage at various stages of growth, as ECM development correlates strongly with the developing tissue's mechanical properties.[39] First, extensive biochemical and histologic characterizations were performed. Samples were removed from cultures containing 10% and 20% FBS at 2, 4, 6, 8 and 10 weeks and frozen to measure DNA content of the neocartilage and for biochemical evaluation of the ECM (See Supporting Information). ECM accumulation in the constructs was evaluated by quantifying the amount of two important components of ECM: 1) hydroxyproline (HYP) as a marker of collagen content, and 2) sulfated glycosaminoglycan (GAG) as a marker of proteoglycans. By week 10, the HYP content increased to 1.2 ± 0.1 μg/mg and 1.4 ± 0.2 μg/mg for cultures containing 10% and 20% FBS, respectively (Fig. 3A). The corresponding values of GAG content for week 10 were 10.6 ± 0.6 μg/mg and 12.2 ± 1.0 μg/mg (Fig. 3B). This increase in GAG and HYP content indicates that chondrocytes are alive and metabolically active in culture.

Next, tensile properties were analyzed by testing 3D printed chondrocyte-alginate dogbone samples at various points in culture, in which the dogbones contained the same cell densities and identical culturing conditions as the ear (See Supporting Information). Evaluation of the mechanical properties indicated that the Young's modulus of the dogbones increased with time from 14.16 kPa to 111.46 kPa at week 10 (Fig. 3C). Dogbones of a lower chondrocyte density of 20 million cells/mL were also tested under similar conditions to understand the effect of the initial chondrocyte density in the mechanical properties of the grown tissue. These were found to possess a lower Young's modulus of 73.26 kPa at week 10. Next, the hardness of the grown cartilaginous tissue of the 3D printed auricle was characterized using nanoindentation measurements. The indentations were performed at the various anatomic sites of the auricle (Fig. 3D). As shown in Table 1, these hardness values were found to be relatively uniform, ranging from 38.50 kPa to 46.80 kPa, confirming the structural integrity of the printed ear.[40]

To demonstrate the enhanced functionalities of the 3D printed bionic ear, we performed a series of electrical characterizations. First, the resistivity of the coil antenna was measured using four point probe measurements and found to be dependent on the volumetric flow rate used for printing the conducting AgNP-infused silicone (See Supporting Information). At

the optimum flow rate, the resistivity of the printed coil was found to be 1.31×10^{-6} Ω·m, which is only two orders of magnitude higher than pure silver (1.59×10^{-8} Ω·m). Next, we performed wireless radio frequency reception experiments. To demonstrate the ability of the bionic ear to receive signals beyond normal audible signal frequencies (in humans, 20 Hz to 20 kHz), we formed external connections to the cochlea-shaped electrodes stemming from the inductive coil of the bionic ear (Figure 4A). The ear was then exposed to sine waves of frequencies ranging from 1 MHz to 5 GHz. The S21 (forward transmission coefficient) parameter of the coil antenna was analyzed using a network analyzer and was found to transmit signals across this extended frequency spectrum (Fig. 4B).

Most importantly, as a demonstrative example of the versatility in modifying the final organ by modifying the CAD design, we printed a complementary left ear by simply reflecting the original model (see Supporting Information). Left and right channels of stereophonic audio were exposed to the left and right bionic ear via transmitting magnetic loop antennas with ferrite cores (Fig. 4C). The signals received by the bionic ears were collected from the signal output of the dual cochlea shaped electrodes and fed into a digital oscilloscope and played back by a loud speaker for auditory and visual monitoring. Excerpts of the transmitted and received signals of duration 1 ms for both the right and left bionic ears are shown in Figure 4D and are found to exhibit excellent reproduction of the audio signal. Significantly, the played back music (Beethoven's "Für Elise") from the signal received by the bionic ears possessed good sound quality (Movie 2).

In summary, designer "cyborg ears" were fabricated which are capable of receiving electromagnetic signals over an expansive frequency range from Hz to GHz. Our strategy represents a proof of principle of intertwining the versatility of additive manufacturing techniques with nanoparticle assembly and tissue engineering concepts. The result is the generation of *bona fide* bionic organs in both form and function, as validated by tissue engineering benchmarks and electrical measurements. Such hybrids are distinct from either engineered tissue or planar/flexible electronics and offer a unique way of attaining a seamless integration of electronics with tissues to generate "off-the-shelf" cyborg organs. Finally, the use of 3D printing with other classes of nanoscale functional building blocks, including semiconductor, magnetic, plasmonic, and ferroelectric nanoparticles, could expand the opportunities for engineering bionic tissues and organs.

Supplementary Material

Refer to Web version on PubMed Central for supplementary material.

Acknowledgments

We thank Kellye Cung, Yao-Wen Yeh, and Dr. Ismaiel Yakub for valuable discussions and technical assistance. The 3D CAD model of the ear was downloaded from thingiverse.com and was also used to render the ear images in the manuscript (Figures 1a, 1c, 4c, and the TOC image). A student version of the Autodesk 3ds Max software package was used to modify and render the 3D images. Beethoven's Für Elise music was obtained from the online collection created by Jason Shaw with permission through audionautix.com. Released under Creative Commons License 3.0. Downloadable release form is available at http://www.audionautix.com/Saved/CCrelease.jpg. M.C.M. acknowledges support of this work by the Defense Advanced Research Projects Agency (No. D12AP00245) and the Air Force Office of Scientific Research (No. FA9550-12-1-0367). D.H.G. acknowledges support from the NIH Director's New Innovator program (DP2-OD004346-01). This material is based upon work supported by the Grand Challenges Program at Princeton University.

References

1. Lavine M, Roberts L, Smith O. Science. 2002; 295:995. [PubMed: 11858161]
2. Craelius W. Science. 2002; 295:1018–21. [PubMed: 11834819]

3. Green DW. Biomed Mater. 2008; 3:034010. [PubMed: 18708710]
4. Tian B, Liu J, Dvir T, Jin L, Tsui JH, Qing Q, Suo Z, Langer R, Kohane DS, Lieber CM. Nat Mater. 2012; 11:986–94. [PubMed: 22922448]
5. Timko BP, Cohen-Karni T, Yu G, Qing Q, Tian B, Lieber CM. Nano Lett. 2009; 9:914–8. [PubMed: 19170614]
6. Nguyen TD, Deshmukh N, Nagarah JM, Kramer T, Purohit PK, Berry MJ, McAlpine MC. Nat Nanotech. 2012; 7:587–93.
7. Viventi J, Kim DH, Vigeland L, Frechette ES, Blanco JA, Kim YS, Avrin AE, Tiruvadi VR, Hwang SW, Vanleer AC, Wulsin DF, Davis K, Gelber CE, Palmer L, Van der Spiegel J, Wu J, Xiao J, Huang Y, Contreras D, Rogers JA, Litt B. Nat Neurosci. 2011; 14:1599–605. [PubMed: 22081157]
8. Kim DH, Lu N, Ma R, Kim YS, Kim RH, Wang S, Wu J, Won SM, Tao H, Islam A, Yu KJ, Kim TI, Chowdhury R, Ying M, Xu L, Li M, Chung HJ, Keum H, McCormick M, Liu P, Zhang YW, Omenetto FG, Huang Y, Coleman T, Rogers JA. Science. 2011; 333:838–43. [PubMed: 21836009]
9. Mannoor MS, Tao H, Clayton JD, Sengupta A, Kaplan DL, Naik RR, Verma N, Omenetto FG, McAlpine MC. Nat Commun. 2012; 3:763. [PubMed: 22453836]
10. Pampaloni F, Reynaud EG, Stelzer EH. Nat Rev Mol Cell Biol. 2007; 8:839–45. [PubMed: 17684528]
11. Langer R, Vacanti JP. Science. 1993; 260:920–6. [PubMed: 8493529]
12. Langer R, Vacanti JP. Sci Am. 1995; 273:130–3. [PubMed: 7652530]
13. Jayawarna V, Ali M, Jowitt TA, Miller AF, Saiani A, Gough JE, Ulijn RV. Adv Mater. 2006; 18:611–614.
14. Lee MY, Kumar RA, Sukumaran SM, Hogg MG, Clark DS, Dordick JS. Proc Natl Acad Sci USA. 2008; 105:59–63. [PubMed: 18160535]
15. Mapili G, Lu Y, Chen S, Roy K. J Biomed Mater Res B Appl Biomater. 2005; 75:414–24. [PubMed: 16025464]
16. Marler JJ, Upton J, Langer R, Vacanti JP. Adv Drug Delivery Rev. 1998; 33:165–182.
17. Shieh SJ, Terada S, Vacanti JP. Biomaterials. 2004; 25:1545–57. [PubMed: 14697857]
18. Napolitano AP, Dean DM, Man AJ, Youssef J, Ho DN, Rago AP, Lech MP, Morgan JR. BioTechniques. 2007; 43:494, 496–500. [PubMed: 18019341]
19. Jamal M, Kadam SS, Xiao R, Jivan F, Onn TM, Fernandes R, Nguyen TD, Gracias DH. Adv Healthcare Mater. 2013
20. Chang SC, Tobias G, Roy AK, Vacanti CA, Bonassar LJ. Plast Reconstr Surg. 2003; 112:793–9. [PubMed: 12960860]
21. Khademhosseini A, Langer R, Borenstein J, Vacanti JP. Proc Natl Acad Sci USA. 2006; 103:2480–7. [PubMed: 16477028]
22. Atala A. Curr Opin Biotechnol. 2009; 20:575–92. [PubMed: 19896823]
23. Cao Y, Vacanti JP, Paige KT, Upton J, Vacanti CA. Plast Reconstr Surg. 1997; 100:297–302. discussion 303–4. [PubMed: 9252594]
24. Symes MD, Kitson PJ, Yan J, Richmond CJ, Cooper GJ, Bowman RW, Vilbrandt T, Cronin L. Nature Chem. 2012; 4:349–54. [PubMed: 22522253]
25. Jones N. Nature. 2012; 487:22–3. [PubMed: 22763531]
26. Reiffel AJ, Kafka C, Hernandez KA, Popa S, Perez JL, Zhou S, Pramanik S, Brown BN, Ryu WS, Bonassar LJ, Spector JA. PLoS One. 2013; 8:e56506. [PubMed: 23437148]
27. Villar G, Graham AD, Bayley H. Science. 2013; 340:48–52. [PubMed: 23559243]
28. Yeong WY, Chua CK, Leong KF, Chandrasekaran M. Trends Biotechnol. 2004; 22:643–52. [PubMed: 15542155]
29. Cohen DL, Malone E, Lipson H, Bonassar LJ. Tissue Eng. 2006; 12:1325–35. [PubMed: 16771645]
30. Khalil S, Nam J, Sun W. Rapid Prototyping J. 2005; 11:9–17.
31. Xu T, Binder KW, Albanna MZ, Dice D, Zhao W, Yoo JJ, Atala A. Biofabrication. 2013; 5:015001. [PubMed: 23172542]
32. Malone E, Berry M, Lipson H. Rapid Prototyping J. 2008; 14:128–140.

33. Ahn BY, Duoss EB, Motala MJ, Guo X, Park SI, Xiong Y, Yoon J, Nuzzo RG, Rogers JA, Lewis JA. Science. 2009; 323:1590–3. [PubMed: 19213878]
34. Wu W, DeConinck A, Lewis JA. Adv Mater. 2011; 23:H178–83. [PubMed: 21438034]
35. Someya T, Sekitani T, Iba S, Kato Y, Kawaguchi H, Sakurai T. Proc Natl Acad Sci USA. 2004; 101:9966–70. [PubMed: 15226508]
36. Bichara DA, O'Sullivan NA, Pomerantseva I, Zhao X, Sundback CA, Vacanti JP, Randolph MA. Tissue Eng Pt B Rev. 2012; 18:51–61.
37. Marijnissen WJCM, van Osch GJVM, Aigner J, van der Veen SW, Hollander AP, Verwoerd-Verhoef HL, Verhaar JAN. Biomaterials. 2002; 23:1511–1517. [PubMed: 11833491]
38. Dobratz EJ, Kim SW, Voglewede A, Park SS. Arch Facial Plast Surg. 2009; 11:40–47. [PubMed: 19153292]
39. Kelly DJ, Crawford A, Dickinson SC, Sims TJ, Mundy J, Hollander AP, Prendergast PJ, Hatton PV. J Mater Sci Mater Med. 2007; 18:273–81. [PubMed: 17323158]
40. Li C, Pruitt LA, King KB. J Biomed Mater Res A. 2006; 78:729–38. [PubMed: 16739105]

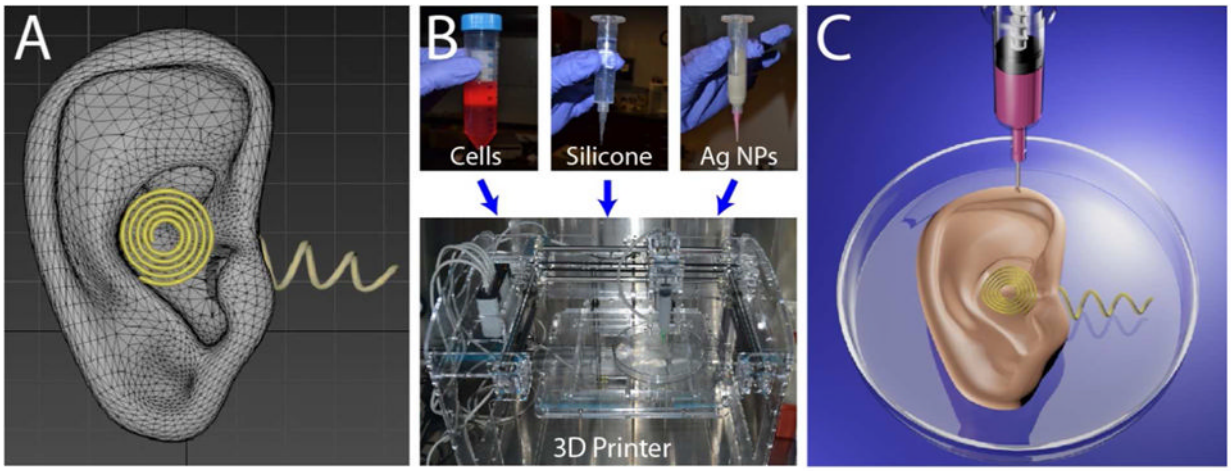

Figure 1.
Three-dimensional interweaving of biology and electronics via additive manufacturing to generate a bionic ear. (**A**) CAD drawing of the bionic ear. (**B**) (top) Optical images of the functional materials, including biological (chondrocytes), structural (silicone), and electronic (AgNPinfused silicone) used to form the bionic ear. (bottom) a 3D printer used for the printing process. (**C**) Illustration of the 3D printed bionic ear.

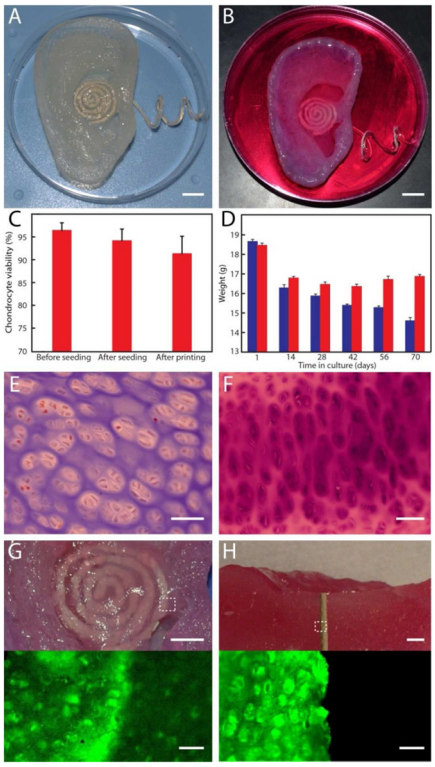

Figure 2.

Growth and viability of the bionic ear. (**A**) Image of the 3D printed bionic ear immediately after printing. (**B**) Image of the 3D printed bionic ear during *in vitro* culture. Scale bars in (**A**) and (**B**) are 1 cm. (**C**) Chondrocyte viability at various stages of the printing process. Error bars show standard deviation with N=3. (**D**) Variation in the weight of the printed ear over time in culture, where the ear consists of chondrocyte-seeded alginate (red) or only alginate (blue). Error bars show standard deviation with N=3. (**E**) Histologic evaluation of chondrocyte morphology using H&E staining. (**F**) Safranin O staining of the neocartilaginous tissue after 10 weeks of culture. (**G**) Photograph (top) and fluorescent (bottom) images showing viability of the neocartilaginous tissue in contact with the coil antenna. (**H**) Photograph (top) and fluorescent (bottom) images of a cross section of the bionic ear showing viability of the internal cartilaginous tissue in contact with the electrode. Top scale bars are 5 mm; bottom are 50 μm.

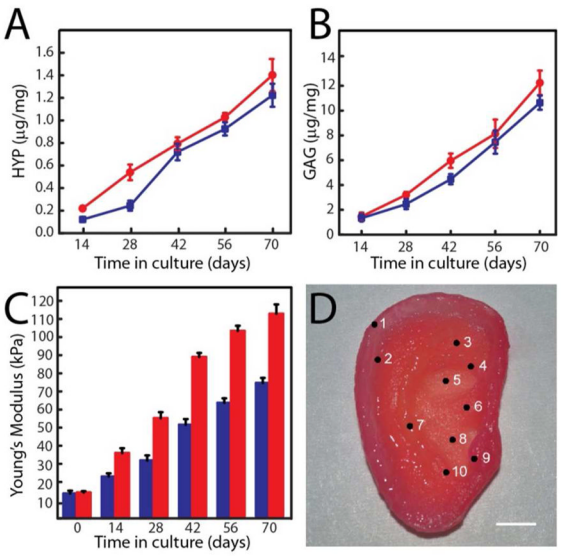

Table 1

Part	Mean Hardness (kPa)
1. Helix	44.85 ± 2.68
2. Scapha	38.93 ± 3.00
3. Fossa	42.40 ± 2.87
4. Crura Antihelix	45.47 ± 3.95
5. Cymba Conchae	41.53 ± 4.36
6. Crus of Helix	46.80 ± 4.72
7. Antihelix	40.67 ± 3.13
8. Cavum Conchae	38.50 ± 1.73
9. Tragus	40.10 ± 2.42
10. Antitragus	39.27 ± 3.26

Figure 3.

Biomechanical characterization of the 3D printed neocartilage tissue. (**A**) Variation of HYP content over time in culture with 20 % (red) and 10 % (blue) FBS. (**B**) Variation of GAG content over time in culture with 20 % (red) and 10 % (blue) FBS. (**C**) Variation of Young's modulus of 3D printed dog bone constructs over time in culture with 20 million (blue) and 60 million (red) cells/mL. Error bars for parts A-C show standard deviation with N=3. (**D**) Various anatomic sites of the ear auricle, with corresponding hardness listed in Table 1. Scale bar is 1 cm.

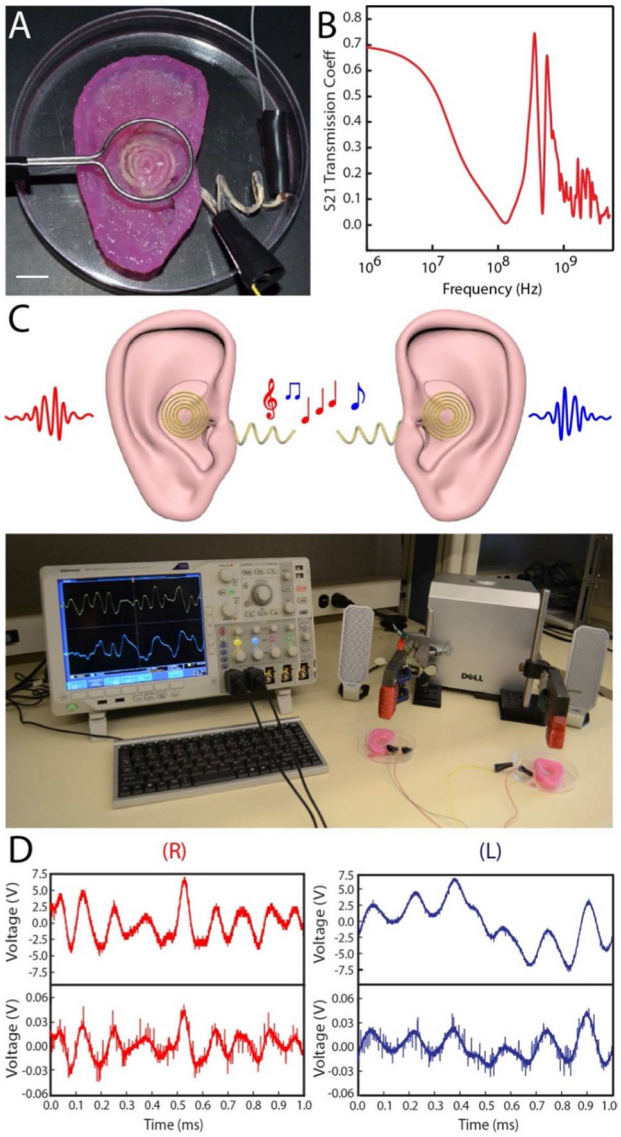

Figure 4.

Electrical characterization of the bionic ear. (**A**) Image of the experimental setup used to characterize the bionic ear. The ear is exposed to a signal from a transmitting loop antenna. The output signal is collected via connections to two electrodes on the cochlea. Scale bar is 1 cm. (**B**) Response of the bionic ear to radio frequencies in terms of S21, the forward power transmission coefficient. (**C**) (top) Schematic representation of the radio signal reception of two complementary (left and right) bionic ears. (bottom) Photograph of complementary bionic ears listening to stereophonic audio music. (**D**) Transmitted (top) and received (bottom) audio signals of the right (R) and left (L) bionic ears.

Table 1

Part	Mean Hardness (kPa)
1. Helix	44.85 ± 2.68
2. Scapha	38.93 ± 3.00
3. Fossa	42.40 ± 2.87
4. Crura Antihelix	45.47 ± 3.95
5. Cymba Conchae	41.53 ± 4.36
6. Crus of Helix	46.80 ± 4.72
7. Antihelix	40.67 ± 3.13
8. Cavum Conchae	38.50 ± 1.73
9. Tragus	40.10 ± 2.42
10. Antitragus	39.27 ± 3.26